Measurement of fatigue crack deformation on the macro- and micro-scale: uniform and non-uniform loading

S.J. O'Connor, D. Nowell*, and K.I. Dragnevski
University of Oxford, Department of Engineering Science,
Parks Road, Oxford, OX1 3PJ, UK
**Corresponding author: david.nowell@eng.ox.ac.uk*

Abstract

This paper describes the experimental measurement of near-tip displacement fields for a fatigue crack growing in a small compact-tension specimen. The specimen is pre-cracked conventionally, but then loaded in-situ in a scanning electron microscope. Digital image correlation is applied to the images collected and is analysed using an elastic model to produce stress intensity factor histories. A simple elastic/plastic model due to Pommier and Hamam is also applied, and the resulting behaviour is discussed. A single overload is applied to the specimen, and the effect of this on the elastic and elastic-plastic results is examined. The results are also compared to earlier work of a similar nature using a long-distance microscope, which gives an understanding of crack behaviour at a macroscopic length scale.

Keywords: Crack Tip Displacements, Digital Image Correlation, Elastic-Plastic Fracture Mechanics, Overload.

1. Introduction

An understanding of fatigue crack propagation is an essential pre-requisite to safe operation of many engineering structures and systems. Most damage tolerant life prediction approaches are based on the application of experimental crack propagation data to the real system. For example, the Paris Law [1] is frequently used to apply experimental da/dN vs delta K data to service loads and to the system geometry. However, most experimental data is obtained for constant amplitude loading whereas engineering systems frequently experience non-uniform loading. The presence of history effects in fatigue crack propagation is well known and this means that life prediction under service loading conditions remains a challenging problem in many cases. A detailed understanding of the crack tip response to a range of load histories is the key to improvements in this area.

Previous experimental work on crack tip behaviour has been wide-ranging. Photoelasticity was used in early investigations (e.g. [2]). Indeed, before the advent of finite element analysis, this was the principal method of determining stress intensity factors for cracks in anything other than simple geometries. Transmission photoelasticity suffers from the drawback (particularly as far as fatigue cracks are concerned), that the material behaviour in the process zone will differ from that in the main classes of engineering materials. Reflection photoelasticity can, of course, be used to circumvent this, but is more complex experimentally [3]. Other experimental techniques employed have included caustics [4], interferometry [5], and point measurements with strain gauges [6]. The last decade has

seen the widespread adoption of digital image correlation (DIC) [7] as a practical tool in experimental mechanics. It was not long before this was applied to the analysis of crack behaviour [8], including that of fatigue cracks [9]. Digital volume correlation of tomographic images has also been employed to produce 3D data [10], but at present it is limited to very small samples in materials of practical engineering interest.

Particularly interesting are studies which use DIC to examine behaviour close to the crack tip, including closure. The first recorded work of this nature in the literature was that of Sutton et al [11] in 1997. Very little further work was reported until the late 2000s, when a number of investigations took place, including [9], [12], and [13]. Our own recent work at Oxford has been presented at the Forni di Sopra [14],[15] Malaga [16], and Urbino [17] IJ Fatigue/FFEMS workshops and has concentrated on the use of digital image correlation to measure and analyse the displacements fields around a crack tip. Our experiments have made use of a long-range optical microscope to examine deformations in a region within 0.5 mm of the crack tip. Analysis of these deformations has allowed stress intensity factors to be calculated and crack closure assessed [18]. In the current paper we will seek to extend this approach by reporting measurements taken during in-situ loading of a fatigue crack in a scanning electron microscope. This permits more detailed examination of the displacement field in the neighbourhood of the crack tip.

2. Macroscopic Measurements

Our earlier work on the measurement of crack tip displacement fields has employed a long range microscope, focused on an area approximately 600 x 400 μm close to the crack tip [14] in a compact tension specimen. A number of images were captured at intervals during the loading cycle, and digital image correlation carried out using a public domain Matlab script produced by Erbl et al [19]. The reference image (where zero displacement is assumed) was taken at minimum load, in this case 10% of the maximum (R = 0.1). The data obtained were processed in a number of ways, but a particularly convenient means of presenting the results is to determine the experimental stress intensity factor by comparing the measured crack tip opening displacements with those predicted by an elastic model. The crack flank displacements for an elastic crack are given by

$$u_i = \pm\frac{4K_I}{E}\sqrt{\frac{r}{2\pi}}u_i = \pm\frac{4K_I}{E}\sqrt{\frac{r}{2\pi}} \quad (1)$$

where K_I is the elastic stress intensity factor, E is Young's Modulus, and r is the distance from the crack tip. Hence, a plot of u_i against $\sqrt{r}$ should yield a straight line and the stress intensity factor can be extracted from the gradient. Alternatively, a plot of $log(u_i)$ against $log(r)$ should give a straight line fit with a slope of 0.5. K may then be obtained from the intercept. Figure 1(a) shows results from a typical experiment conducted under constant amplitude loading. The dotted line represents the theoretical variation of elastic stress intensity factor with load for the size and type of specimen used (a standard Compact Tension specimen). It will be seen that the experimental results broadly follow the theoretical ones, and that the slope of the load vs K line is very similar. However the experimental results exhibit an offset, and the experimental K values are lower than predicted. This may be interpreted as being due to plasticity induced crack closure, which causes superposition of an additional negative residual K term (K_r). It can be seen from the results that the crack does not open until about 0.5kN of applied load (approximately 25% of the maximum load).

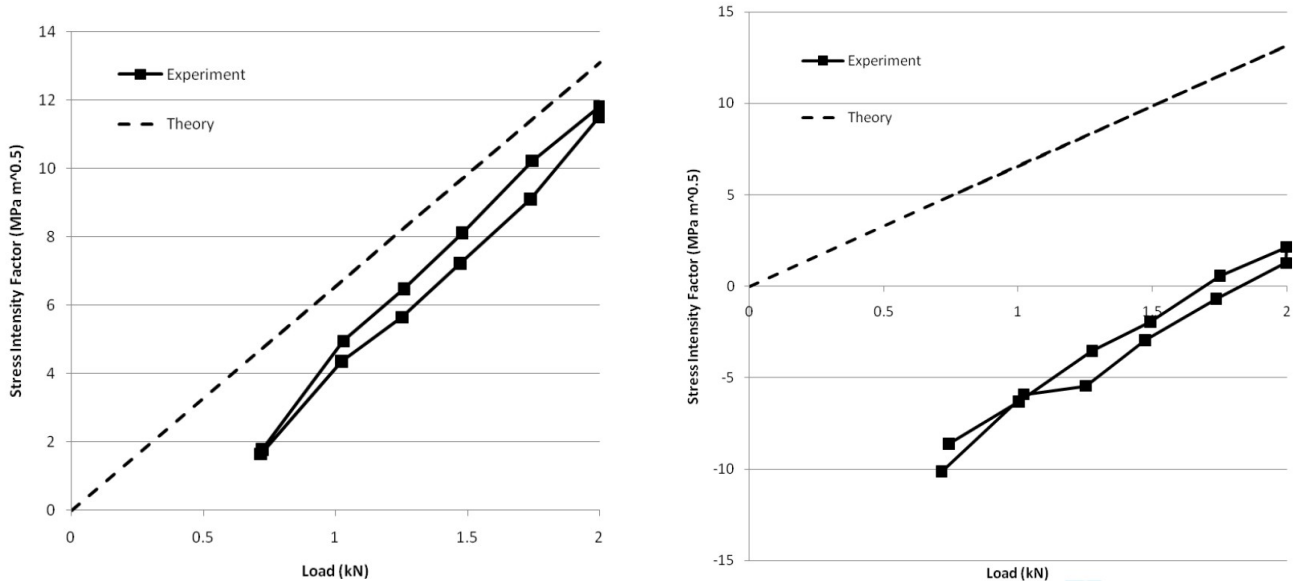

Figure 1: Macroscopic results: variation of measured stress intensity factor with load for specimen CTF6 [16] (a) After constant amplitude loading and (b) Immediately after an overload.

Figure 1(b) shows results from the same specimen immediately after a 50% overload cycle. Although the slope of the experimental line remains parallel to the theoretical one, these results exhibit some unusual features. In particular, negative K values are measured, which at first sight appears physically unreasonable. However, if there is a large plastic opening displacement at the crack tip, a crack shape of this form is possible, and closer inspection of the experimental results suggests that this is the measured deformation. In other words, the crack experiences significant

blunting, and almost all of the unloading may be treated as elastic, with the crack fully open. Hence, the delta K experienced by the crack tip may be larger on unloading from the overload than on loading (when closure is present) and negative K may be measured. The results presented here were obtained by analysing the relative displacement of 5 pairs of points from the recorded images, and the first pair is approximately 100 μm from the crack tip. In order to investigate the crack tip deformation in more detail, a novel experiment was therefore proposed, which involved in-situ loading of a small specimen in the scanning electron microscope.

3. Microscopic Measurements

Experiments were conducted in the Laboratory for In-situ Microscopy and Analysis (LIMA), which is part of the Solid Mechanics and Materials Engineering Group at the University of Oxford. The imaging device used was a Carl Zeiss Evo LS15 VP-Scanning Electron Microscope. The following imaging parameters were used: Electron High Tension: 15kV; working distance in the region of 10mm; imaging carried out using Secondary Electron Detector; probe current (which defines the spot size) 310pA; scan time: 10.2 sec. The standard Zeiss pre-set line integration was used for image integration. The above parameters provided stable imaging conditions throughout the duration of the experiments. The chamber of the SEM was large enough so that in-situ testing could be performed with a Deben testing stage similar to that shown in Figure 2. A 5 kN load cell was attached to the testing stage and an extension rate of 1:25 mm/min was used for this testing. Computer software was used to set the drive parameters and to collect live data on the force applied and extension from the testing stage during loading. The specimen design was a modified compact tension specimen of overall dimensions 35.0 x 33.6 x 3.0 mm (Fig.3). The material used was 6082-T6 aluminium alloy with a Young's modulus of 70 GPa, a yield stress of approximately 320 MPa, and a UTS of 330 MPa. This was the same as that used in the earlier macroscopic tests. Cyclic properties were not measured, but this alloy exhibits a small amount of cyclic softening or hardening depending on the strain amplitude [20].

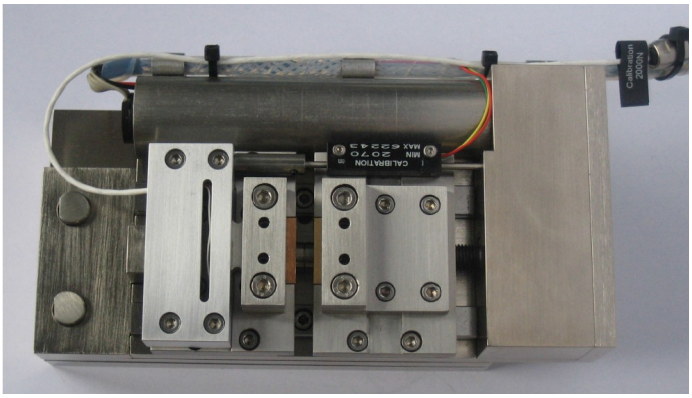

Figure 2: Deben In-Situ Microtest tensile & compression stage.

The specimen was pre-cracked before being loaded on the Deben stage with the same tensile testing rig used for macroscopic specimen loading. For the pre-cracking, the specimen was loaded at a frequency of 5 Hz, significantly faster than could be achieved with the Deben testing stage. 17,000 cycles were applied to the specimen to grow the crack approximately 7mm at the same loads to be used for later testing on the Deben stage. Once pre-cracked and placed on the Deben testing stage, the crack was grown for another 650 cycles to approximately 7.2mm in length before in-situ SEM images were captured. The maximum applied load was 1.25 kN and the minimum load was 0.125 kN, giving an R ratio of 0.1.

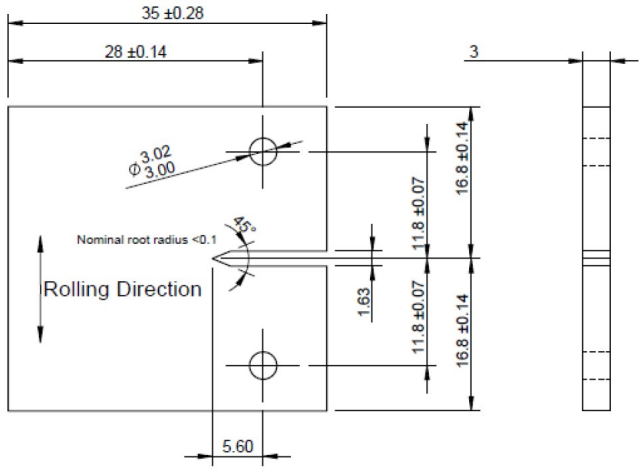

Figure 3: Dimensions (in mm) of specimens used for in-situ SEM testing.

Imaging was carried out using a secondary electron detector at an operating voltage of 15kV and working distance of 9mm and images were captured at a resolution of 3072 x 2304 pixels over an image area of approximately 215 μm x 161 μm. Images were taken every 0.125 kN to give 19 images for a complete cycle of loading and unloading. The images were taken with the crack in approximately the same location within the image. To do this, the load was held

at the desired value while the microscope stage and the electron beam were aligned with the crack before the next image was captured.

Once images were collected, a series of sets of points were selected on either side of the crack and relative displacement was obtained using the DIC algorithm [19] for pairs of points within each set. Each set of points contained 2000 points (with 200 points in the horizontal x direction and 10 in the y direction), see Figure 4. The procedure adopted therefore produced relative displacement in the y direction at 200 different x-direction distances along the crack from the crack tip for each image. The points were distributed from close to the crack tip up to a distance of approximately 150 μm along the crack flanks. Displacement data could have been obtained with fewer points, however a large number of points was selected to reduce the chance that badly tracked points may influence the results. Due to the high resolution of the images, displacements around the crack were quite large at high loads when measured in pixels. Therefore, in order to better track the points, the area surrounding each point that is used for image correlation was increased from a 30 x 30 pixel square used in earlier work up to a 200 x 200 pixel area.

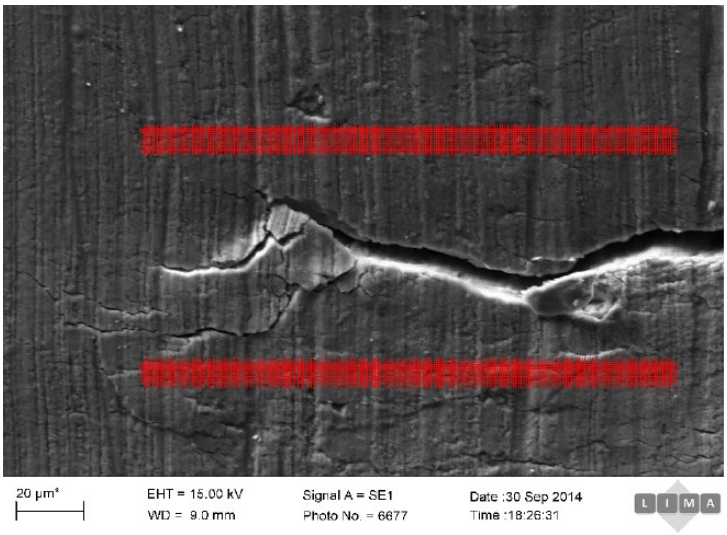

Figure 4: Typical image collected from the experiment at a load of 1.25 kN. Sets of points are selected on either side of the crack to measure relative displacement.

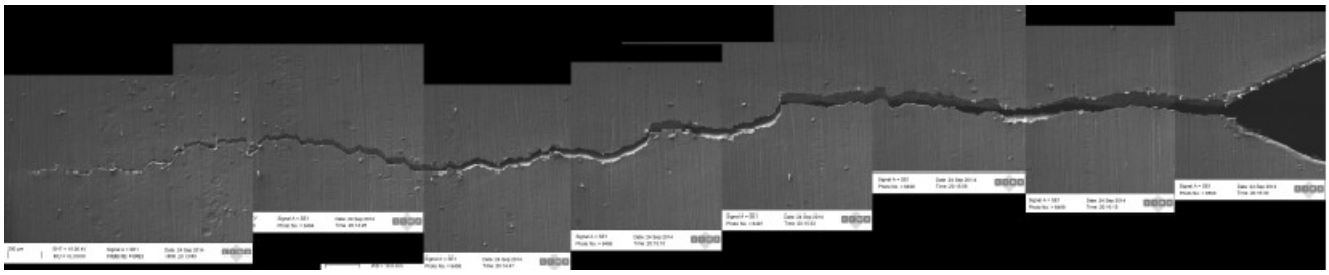

Figure 5: Series of images aligned to give an image of the full crack length at a load of 1.25 kN

In addition to the images taken to analyse displacements around the crack tip, images of the full crack were captured in order to measure crack length for calculation of K. The loading was paused at the highest load of a loading cycle (1.25 kN), magnification reduced and a series of images taken along the full crack. These images were then fitted together using normalised 2-D cross-correlation with the Matlab Image Processing Toolbox to give an image of the full crack in order to measure the total length. An example is shown in Figure 5.

In interpreting the results of the experiment, it is important to consider the various potential sources of error. There are relatively few papers in the literature where DIC is applied to SEM images, and even fewer discuss potential errors. However, Kammers and Daly [21] discuss measurements of strain in a metallic continuum without macroscopic flaws, and conclude that there are three main sources of error:

(i) Drift distortion - where the image changes during acquisition, perhaps because of stress relaxation, or failure of the loading stage to apply constant load or displacement. Whilst this may be an issue in a full-field application, here we are attempting to measure relative displacement of closely-spaced points either side of the crack. The data for these points is acquired at almost the same time during the scan, hence drift distortion is far less of a problem here than it is for Kammers and Daly. The load was held constant for approximately100s during image capture. The specimen was first repositioned to get the crack tip in approximately the same position within the image (this took ~20s). Following this, image capture took 40-60s.

(ii) Spatial distortion – where the electron optics do not give an undistorted image. Again, since we are measuring relative distortion between closely-spaced points, this is much less of an issue than in a full-field measurement.

(ii) Noise – We have relatively large displacements either side of a discontinuity (the crack). Hence the ‘signal to noise ratio’ is much larger than in a continuum problem, where the displacements are relatively small. Thus noise is also less of an issue than in the Kammers and Daly paper. The random variation in the DIC calculated displacement between adjacent points in the array was of the order of + 0.1μm, and corresponding error bars have been included in the plots of raw results.

As discussed above, an estimate of random error is included in the results plotted here. The amount of any systematic error is more difficult to estimate, and we have not attempted to do so here. More work is required in this area if we are to have confidence in the quantitative results produced by the technique. However, qualitative comparison of behaviour (e.g. before an after an overload) is still possible, and as we shall see, the quantitative results look promising. Hence, mindful that these sources of error may be present, we are able to proceed on the assumption that any errors are likely to be less significant than in [21], although they may be more pronounced than in our previous macroscopic DIC work on cracks, [14] to [17]. Another potential issue is that of stress relaxation. Because of the relatively long imaging time detailed above , any stress relaxation might affect the results. However, there is no suggestion in the literature that this is a significant feature of the behaviour of the current material (Al 6082-T6) at room temperature.

3. Results

3.1 Constant Amplitude loading

Measurements for a full cycle of loading were taken after 17,000 cycles of pre-cracking in the hydraulic rig, followed by 650 cycles in the Deben loading fixture. Figure 6 shows the variation of relative displacement between two of the tracked pairs of points, at 10, 50, and 150 μm away from the nominal crack tip as the load is varied through a complete cycle. The behaviour is very similar to that observed with macroscopic displacements [14]. For each pair of points, there is very little relative displacement until a particular load is reached. This may be associated with crack closure. Once the opening load is exceeded, relative displacement increases until the maximum load, then decreases until a closure load is reached, slightly lower than the opening load. For a given load, displacements during unloading are larger than those during loading, due to plastic hysteresis in the crack tip process zone. It is clear from Figure 6 that the opening load is higher for points closer to the crack tip. Hence, the crack peels open from the mouth towards the tip in the same manner as observed with the macroscopic technique.

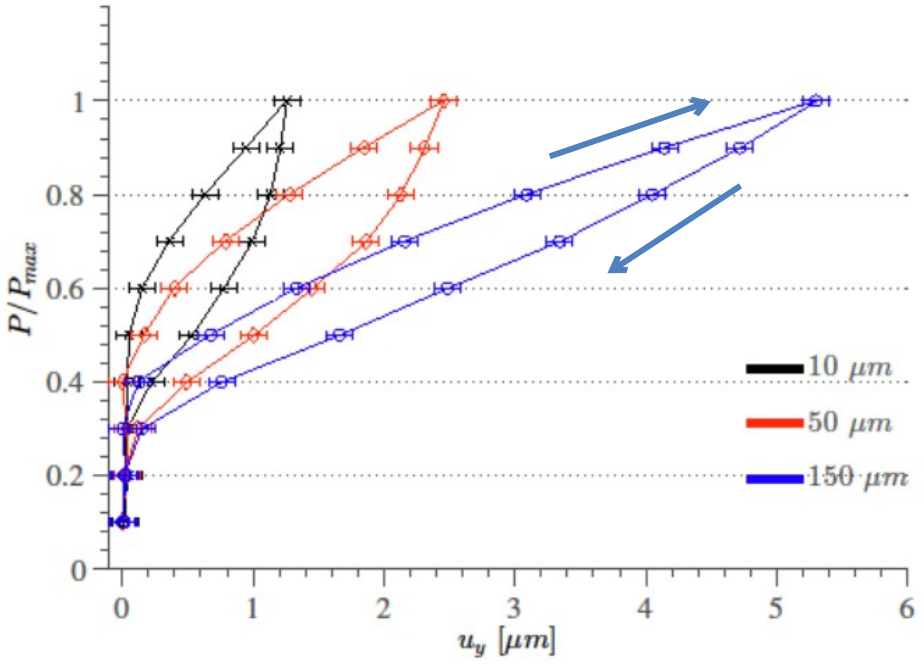

Figure 6. Relative displacement between three pairs of points: 10, 50, and 150 μm away from the nominal crack tip.

As shown in equation (1), if an elastic model is assumed, a plot of log u_y vs. log r should be expected to give a straight line with a gradient of 0.5. This can then be used to obtain an experimental measurement of K from the intercept. However, a more accurate procedure is to plot u_y vs. $\sqrt{r}$ and to obtain K from the slope. A further refinement is to note that the microscopic measurements are very close to the crack tip and it is no longer entirely appropriate to assume that they are close to the crack flanks (i.e. that the angle θ, between the crack growth direction and the line between the crack tip and the measurement point, is 180°). Hence an improved fit is obtained from the full solution for near-tip displacements [23] :

$$u_i = \pm\frac{2K_I}{E}\sqrt{\frac{r}{2\pi}}\sin\left(\frac{\theta}{2}\right)\left(1+\sin^2\left(\frac{\theta}{2}\right)-\nu\cos^2\left(\frac{\theta}{2}\right)\right)$$

$$u_i = \pm\frac{2K_I}{E}\sqrt{\frac{r}{2\pi}}\sin\left(\frac{\theta}{2}\right)\left(1+\sin^2\left(\frac{\theta}{2}\right)-\nu\cos^2\left(\frac{\theta}{2}\right)\right)$$

(2)

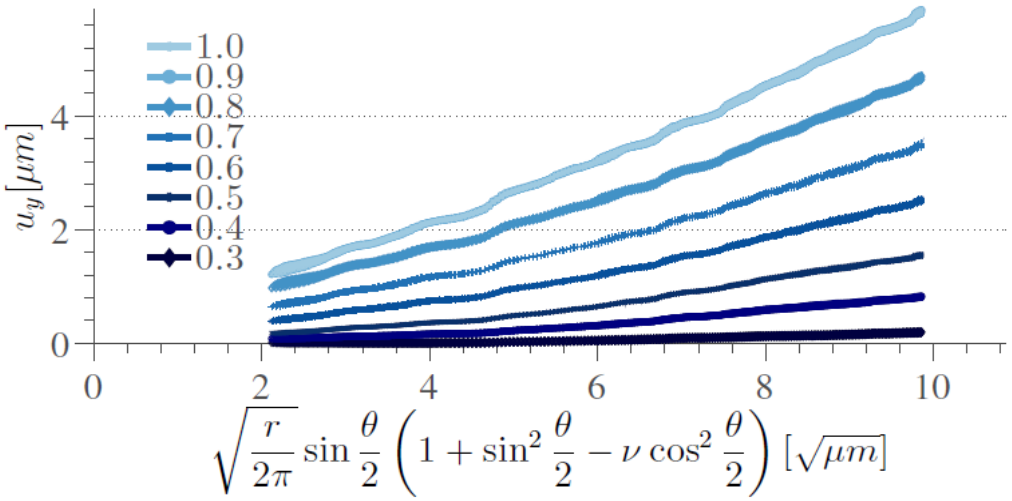

Figure 7. Relative displacements across the crack plotted as a function of $\sqrt{r}$ and corrected for polar angle θ (2) for different values of P/P_{max}

Figure 7 shows a typical set of results plotted in this way and obtained with a crack length (measured from the tip of the starter notch) of approximately 7.2 mm. It will be apparent that the data falls into two distinct sets. Points more than about 25μm from the crack tip seem to give a reasonably good straight line fit. Points closer than 25 μm from the crack tip show a slightly reduced gradient. Nevertheless, all of the data was used to calculate K in the first instance, since it is very difficult to define a precise cut-off value where the deviation from the far field gradient has become significant. The variation of K with load is shown in Figure 8. Also plotted is the theoretical value, calculated from the standard solution for the stress intensity factor in a CT specimen. It will be seen that the results are very similar to those from the macroscopic work (Figure 1a). The gradient of the experimental K vs load curves is about 25% less that for the theoretical line. The discrepancy may be due to an error in the positioning of the crack tip, and this issue will be addressed later. However, more significantly, there is an offset caused by crack closure, so that measured K values are further reduced with respect to the theoretical ones. It should, of course, be remembered that the datum for the DIC measurements is the cracked body with minimum load applied. This will always correspond to a null field and therefore zero K, even though residual displacements will exist when compared with the uncracked body. Nevertheless, the ΔK seen by the crack tip at the surface of the specimen appears to be about half that predicted by linear elastic calculation.

The calculations above seem to show that a linear elastic analysis gives a reasonable fit to the experimental measurements provided that we are more than about 25μm away from the crack tip in the direction of the crack mouth It is instructive to compare this distance with the Irwin [22] estimate of plastic zone size.

$$r_p = \frac{1}{2\pi}\left(\frac{K}{\sigma_y}\right)^2 \quad r_p = \frac{1}{2\pi}\left(\frac{K}{\sigma_y}\right)^2$$

(3)

where σ_y is the yield stress of the material. This gives a figure of $r_p \approx 680$ μm, for the maximum load, although the cyclic plastic zone size will only be about a quarter of this value (170 μm). At first sight this discrepancy in length scales is surprising. However, three factors should be borne in mind:

(i) The datum for the DIC measurement is the cracked body at minimum load, hence, much of the pre-existing displacement would be factored out, and clearly the cyclic plastic zone size is the appropriate one for comparison.

(ii) In plane stress, the plastic zone forms a 'kidney shape', with a cusp at the crack tip [24]. Hence, close to the line of the crack, only material ahead of the crack tip lies in the cyclic plastic zone.

(iii) The cyclic displacements in the crack tip plastic zone are controlled by the surrounding elastic material and hence may not differ significantly from the calculated elastic values.

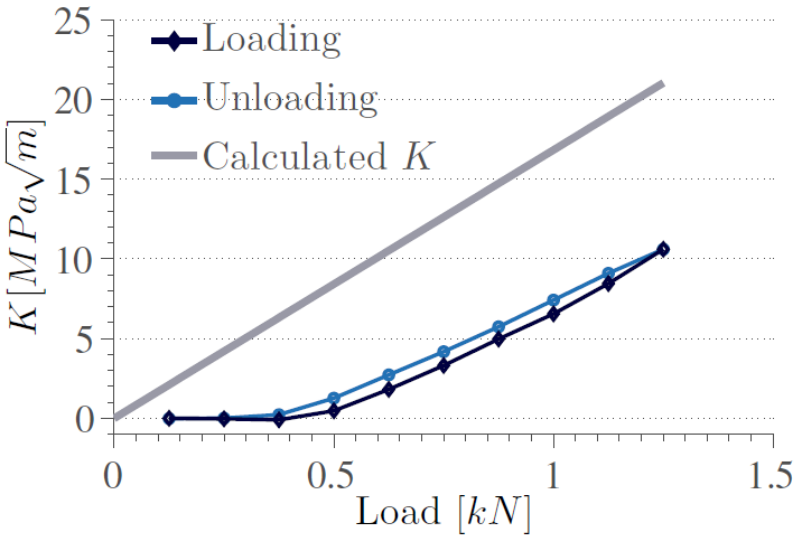

Figure 8. Variation of calculated and measured elastic K with load during one complete loading cycle.

The arguments above suggest that an initial elastic analysis sheds some useful light on the problem. If one considers the Irwin approach [22], a better fit to an elastic model (1) may be obtained by introducing a virtual crack tip, offset

by r_p from the actual tip. However, an elastic/plastic analysis might be argued to be more appropriate at the level of plasticity experienced in the experiment. In common with our earlier work we will choose to employ a model proposed by Pommier and Hamam [25]. This partitions the total displacement field into elastic and plastic components. In terms of displacements along the crack flanks, the model leads to

$$u_y = \frac{8K_I}{E}\sqrt{\frac{r}{2\pi}} + \rho \quad u_y = \frac{8K_I}{E}\sqrt{\frac{r}{2\pi}} + \rho \tag{4}$$

i.e., that a constant plastic displacement component ρ is added to the elastic solution given in equation (1). In practice, of course the plastic deformation at the tip is unlikely to give rise to a constant deformation along the crack flanks, but close to the tip, equation (4) is a reasonable approximation. Plotting u_y against $\sqrt{r}$ should give a straight line with a gradient related to K and an intercept of ρ. Essentially the data is plotted exactly as in Figure 7. Values of K are unchanged, but the intercept is now used to determine ρ.

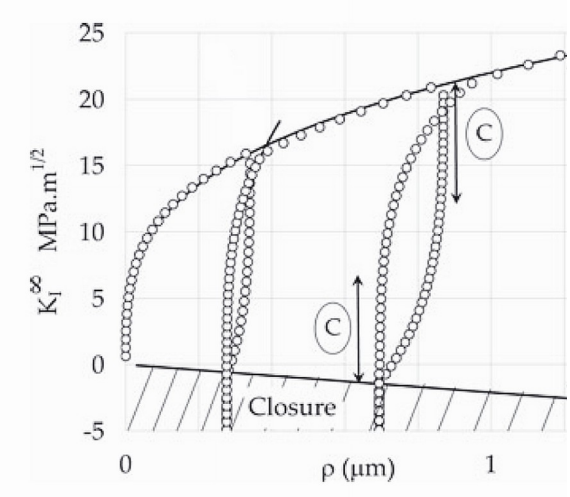

Figure 9. Pommier and Hamam's suggested behaviour in K vs ρ space [25]. Cyclic behaviour is indicated by the loop (C).

Pommier and Hamam [25] concentrate the interpretation of their model on the crack tip behaviour in K vs ρ space. In essence, K may be regarded as the driving force, and ρ represents the process zone response. They have suggested that the relationship between the two parameters should look like that shown schematically in Figure 9. In particular, they suggest that in cyclic loading, such as the loop indicated by (C) in the figure, there is little change in ρ in the first

part of each cycle. This observation can be used to explain the existence of a threshold ΔK in fatigue. It is postulated that, until the application of a certain level of ΔK, there is very little cyclic plasticity (characterised by $\Delta\rho$) and the crack does not grow. The experimental data is plotted in Figure 10a, where it can be seen that the experimental loops are similar in general form to those predicted in [25]. However, there is significant variation in ρ throughout the cycle. In particular, ρ seems to continue to increase for a while after load reversal at maximum load (and similarly decrease for a while at the minimum load reversal). This feature is difficult to explain physically, and may simply be an artefact of the straight line fitting to the u_y vs $\sqrt{r}$ data. This may be seen in Figure 7, where it is clear that fitting a straight line for the data corresponding to P/P_{max} = 0.5 leads to a negative value for ρ. At first sight this may be thought to be physically inadmissible, but it should be remembered that the datum image for the DIC is that at minimum load, rather than corresponding to the undeformed material. Hence, only variations in ρ are measured, not the absolute value so a negative value referred to this datum is not inadmissible. Further, the effect is exaggerated because the reference image is at minimum load in the presence of the crack, rather than the original uncracked body, as is the case, for example, in the diagram in Figure 9. Hence, the relatively small decrease in ρ appears large with respect to the absolute value. Clearly, the effect might result from a measurement inaccuracy, although it is quite consistent across a range of different applied loads. A more likely explanation stems from the approximations present in the model. In particular, that a crack tip opening of ρ is assumed here to cause a constant relative displacement along the crack flanks, whereas in practice it will decrease with increasing distance from the crack tip.

Finally, in Figure 10b, data from two consecutive loading cycles are presented. It will be seen that the cycles are very similar, illustrating the reproducibility of the technique. However, a small increase in ρ can be seen between the first and the second cycle, corresponding to the accumulation of damage at the crack tip and, possibly, crack tip extension. This provides continuum scale evidence of crack tip 'irreversibility', during cyclic loading, similar to that identified at a grain level in recent work by Caroll et al [26].

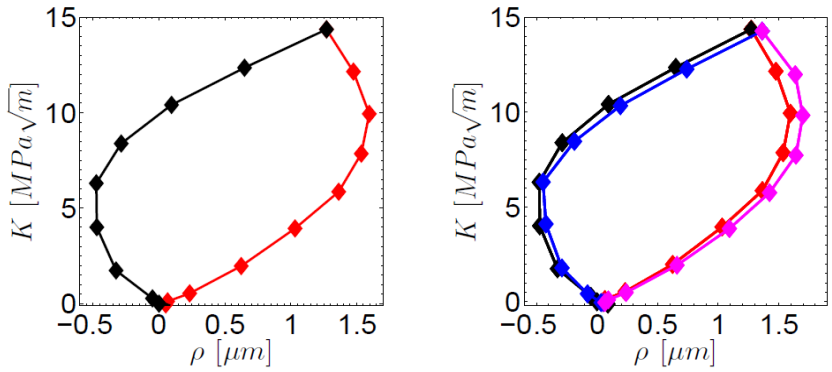

Figure 10. Variation of K and ρ for loading/unloading cycles. (a) Single cycle, loading is on the left of the loop, unloading on the right (b) two consecutive cycles, showing a small increase in ρ between cycles.

3.2 Application of an overload

A single overload cycle was applied to the specimen after 17,764 cycles of constant amplitude loading with the crack grown to 7.18 mm. It proved difficult to track points close to the crack tip during this overload with the DIC method due to significant changes in the images when the load was increased to 150% of the constant amplitude maximum (1.875 kN). A series of images showing the crack tip region during the overload cycle is shown in Figure 11. At the maximum load, the region just ahead of and slightly below the crack tip is heavily plastically deformed. In this region a number of DIC tracking issues occurred. The large amount of deformation meant that the original surface features had changed significantly in appearance. This change to the surface features can be clearly seen in Figure 11c. The displacement of all points around the crack tip during the cycle is displayed in Figure 12 and it is clear from this that some points have been poorly-tracked and need to be removed from further analysis (Fig 12a). The result of removing these points is a remaining selection of points without those within approximately 50 μm of the crack tip (Figure 13). The displacement of the remaining points through a complete cycle is shown in Figure 12b. Some out of plane motion may be apparent in regions of Figure 11. However, we were unable to check explicitly for this (e.g. by back-scattter electron imaging) as it is not possible to tilt the stage with the Deben rig in position. Nevertheless, any effect does not appear to be significant in the regions where DIC is carried out.

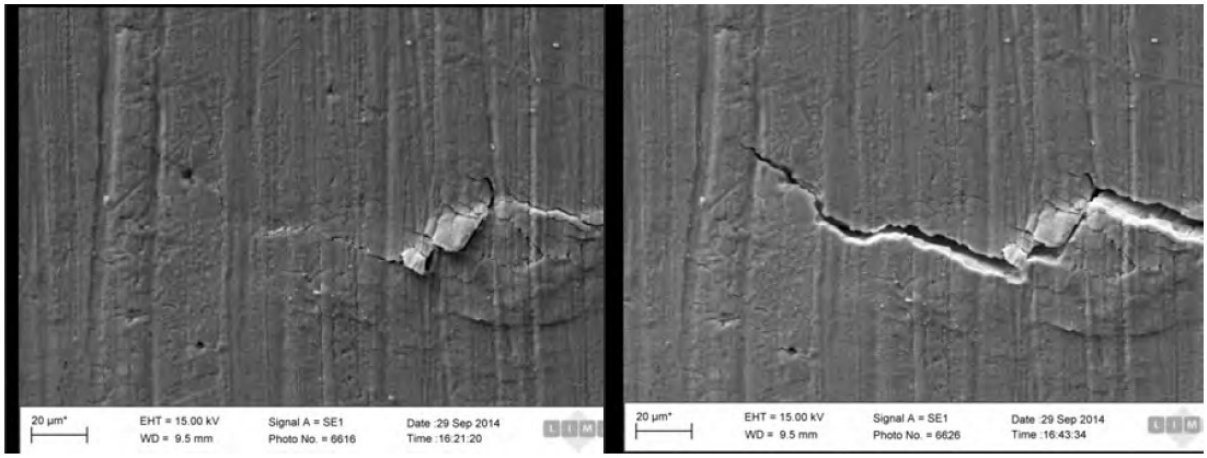

(a) 0.125 kN (b) 1.25 kN

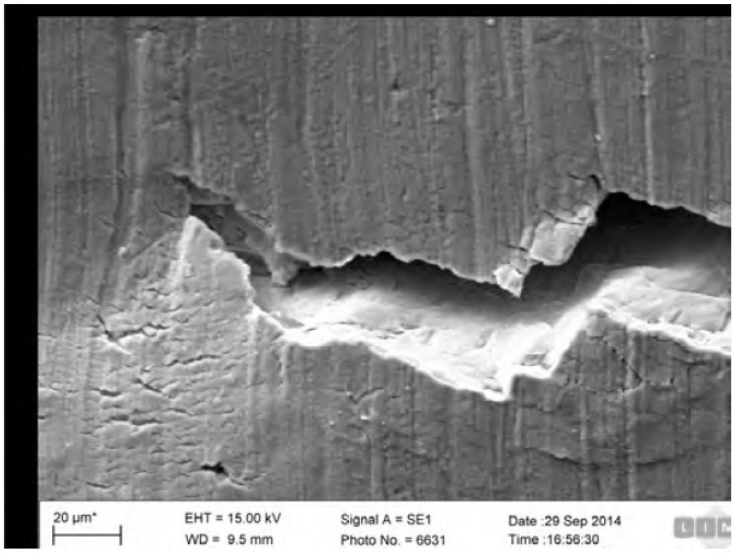

(c) 1.875 kN (overload)

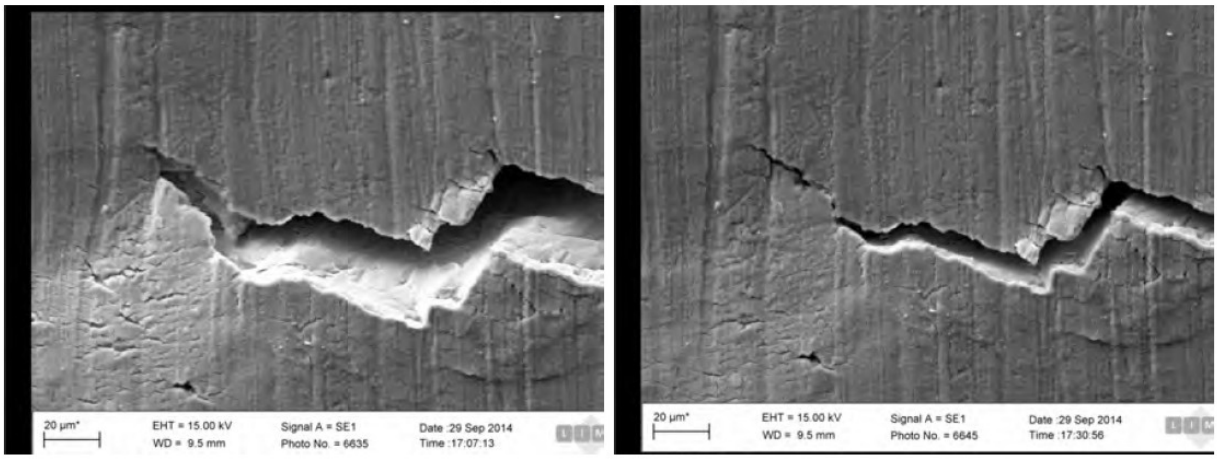

(d) 1.25 kN (unloading) (e) 0.125 kN (unloading)

Figure 11. Series of images taken of the crack tip during a single overload cycle.

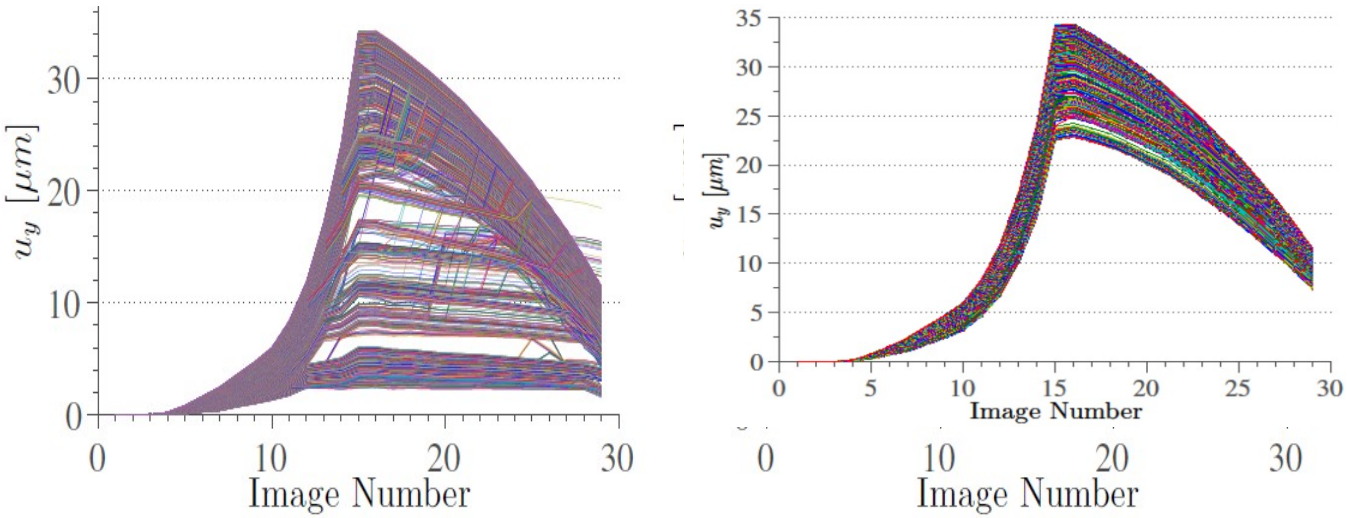

(a) Displacements of all points tracked for an overload cycle

(b) Displacements of points after removing those that were poorly tracked

Figure 12. Plots of the displacement of points around the crack tip for an overload cycle. (a) shows all points, including those which were poorly tracked, (b) shows the points selected for further analysis.

As remarked above, during the overload cycle the crack opens significantly, with large displacements around the crack flanks and a large amount of plastic deformation at the crack tip. The images of the crack tip displayed in Figure 11 show the crack at various stages in this cycle and it is particularly noticeable how much wider the crack is at the overload position (Figure 11c) than at the maximum load during constant amplitude loading (Figure 11b). Relative displacements for two pairs of points close to the crack tip are shown in Figure 14. It can be clearly seen that the magnitude of displacements increases significantly as the load approaches the maximum overload value. In both this figure and in Figure 11 it can be seen that the majority of the crack opening occurs when P/Pmax > 0.66 (i.e. P > 1.25kN, the maximum load during constant amplitude loading). During loading below P/Pmax = 0.66, the displacement values increase almost linearly with increasing load, indicating the relatively small amount of plastic deformation in the cyclic plastic zone. Above the original maximum load there is significant new forward plasticity and this is clearly apparent in the non-linear displacement.

During unloading there is initially very little change in the displacement of the crack flanks. In fact, at 50 µm from the crack tip, the measured displacement actually increases slightly as the load is reduced from 1.875 kN to 1.75 kN. When the load is reduced back to the minimum value of 0.125 kN, considerable residual displacement around the crack remains, Figure 11e. Comparing this image with Figure 11b shows that the residual displacement of the crack

flanks is actually greater after the overload, when the load has been returned to the minimum, than at the maximum load of a constant amplitude loading cycle. A plot of the residual displacement values after the overload is shown in Figure 15, which shows the displacements increasing with distance from the crack tip. This is consistent with measurements of points near the crack tip after an overload in the macroscopic experiment [16], which then showed a decrease in displacements at distances further from the crack tip. In addition to the DIC measurements, the Deben testing stage recorded the extension of the stage during loading of the specimen and a significant residual displacement after the overload was recorded.

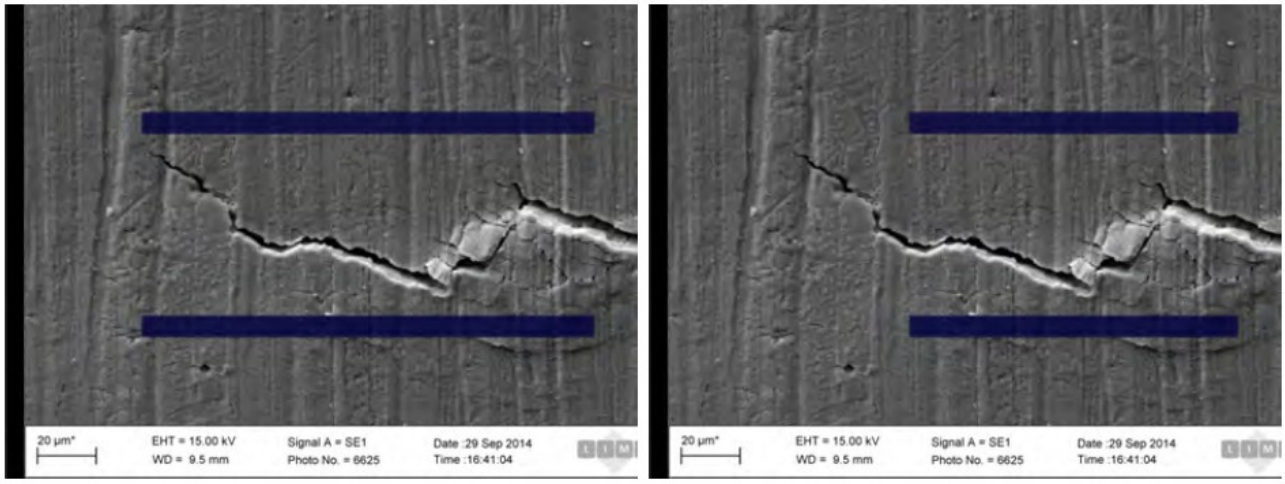

Figure 13. (a) Grid of points initially selected for tracking, and (b) with the poorly-tracked points removed.

Following the application of the overload, the crack was propagated further under the initial loading of 0.125 to 1.25kN. Displacement measurements were taken for the cycle immediately after the over load and at 50, 75, and 125 cycles afterwards. The displacements of all points measured along the crack flanks during constant amplitude loading after the overload were higher than before it. The change in crack closure due to the residual stress at the crack tip is a significant factor in this. Figures 16a and b show relative load vs displacement for the cycle immediately after the overload, and for that 125 cycles later. The reduction in crack closure and the low opening load directly after the overload cycle are immediately apparent in Figure 16a. At this stage, crack closure is very low, as the crack is held open by the residual stress and displacement at the crack tip. Once the crack has grown further, the opening load increases and by 125 cycles afterwards, closure behaviour is similar to that seen before the overload (Figure 16b). There did not seem to be any evidence of increased closure loads after the overload, as was observed in the original

macroscopic experiment [16], but it is possible that the crack had not yet propagated far enough to observe this. In the equivalent macroscopic experiment, approximately 5000 cycles were required before closure levels returned to their original values. Here , we only applied 125 cycles due to the low loading frequency of the Deben rig.

Turning now to the calculated *K*-values, Figure 17a shows the variation of *K* with load for the loading and unloading parts of the overload cycle. It will be seen that the loading curve is almost linear from the point of crack tip opening (0.5kN) until the value of the maximum constant amplitude load (1.25kN). Beyond this, the calculated K increases much more rapidly. This is likely to correspond to the change from relatively modest cyclic plasticity for loads within the constant amplitude range, to creation of a larger zone of forward plasticity for loads above this range. Consequently, it can be concluded that a linear elastic model is a reasonable fit for the constant amplitude loading applied, but not for the overload cycle itself. Unloading from the maximum overload, however, appears to be reasonably linear: once again the crack enters a cyclic plasticity regime, albeit this time from a larger peak load.

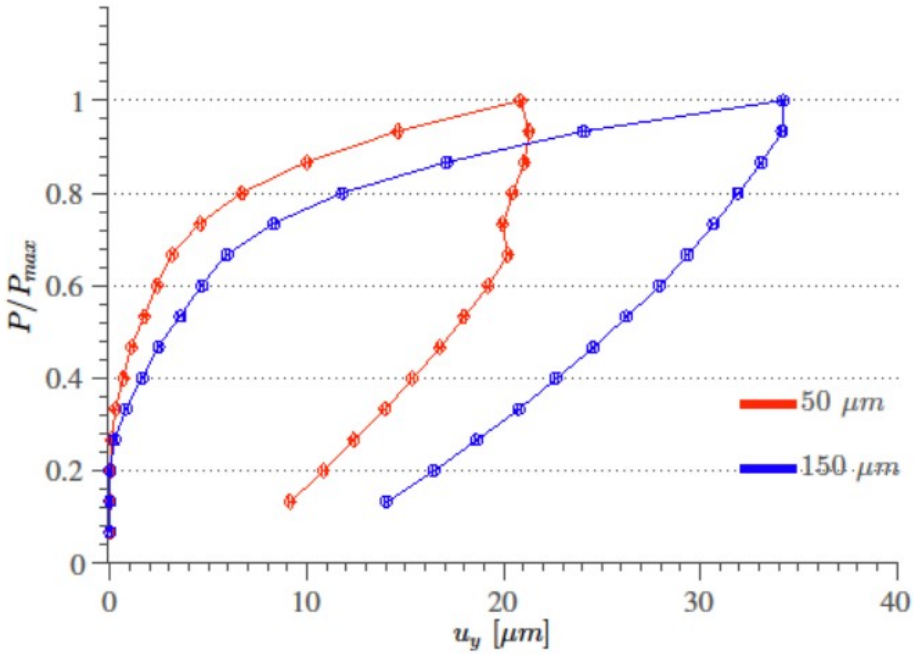

Figure 14. Variation of relative displacement with load during the overload cycle for two pairs of points, located 50 and 100μm from the crack tip.

After the overload cycle, the behaviour of *K* is very similar to what might be expected from looking at the displacement data. The cycle after the overload (Figure 17b) exhibits no features associated with crack closure and therefore is very similar to the calculated value of K, particularly when it is again considered that the datum for DIC

displacements is the minimum load (0.125kN), and this will always correspond to a K of zero by definition. A fairer comparison with theory may be obtained by increasing the experimental measurements by a constant corresponding to the K caused by the minimum load. A further improvement may be made if a shift of 25 μm is made to the assumed position of the crack tip, recognising the argument advanced by Irwin [22] that the elastic model may be better fitted to an elastic-plastic case if the virtual crack tip lies ahead of the real one. The results of applying both these adjustments are shown in Figure 18, where it can be seen that, for the cycle after the overload the theoretical and adjusted experimental K give an extremely good match. The form of the variation of K with load is not substantially affected by the shifted crack tip, including the (lack of) crack closure. However, the assumption does offset the experimental K-values so that they now match the theoretical ones. Finally, Figure 17(c) shows the variation of *K* with load for the cycle applied 125 cycles after the overload. As with the displacement data, the cycle appears to have returned to behaviour similar to the pre-overload value (Figure 8). However, it may be that increases in closure beyond this level would have been observed if the crack had been propagated further after the overload.

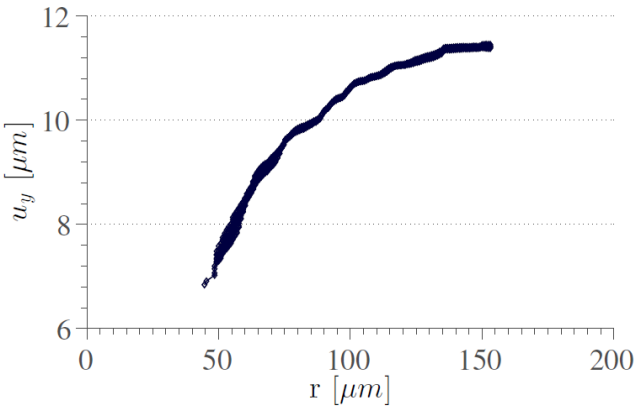

Figure 15. Residual displacement between crack flanks as a function of distance from the crack tip, *r*, at P = 0.125kN, after the application of an overload

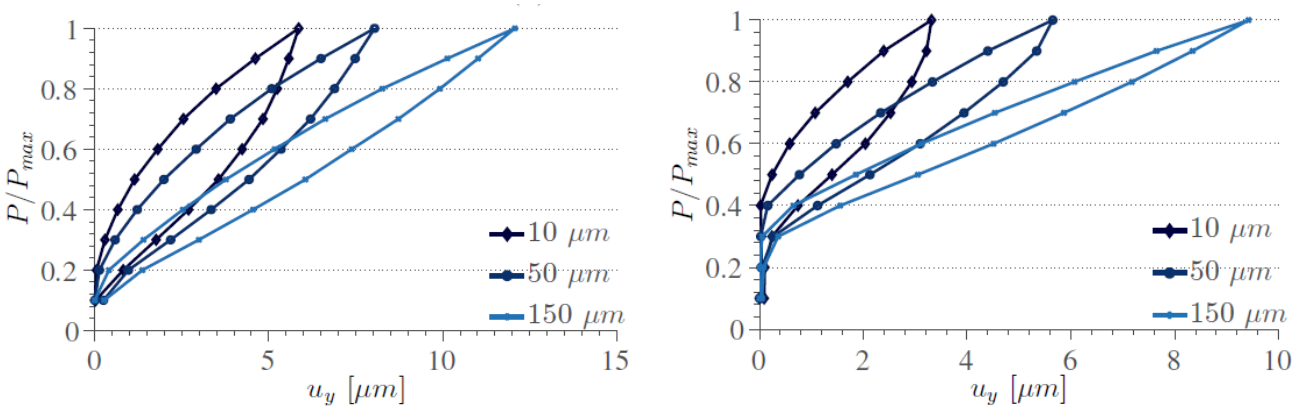

Figure 16. Variation of relative displacement between points at different distances from the crack tip (a) for the cycle immediately after the overload and (b) for the cycle 125 cycles after the overload.

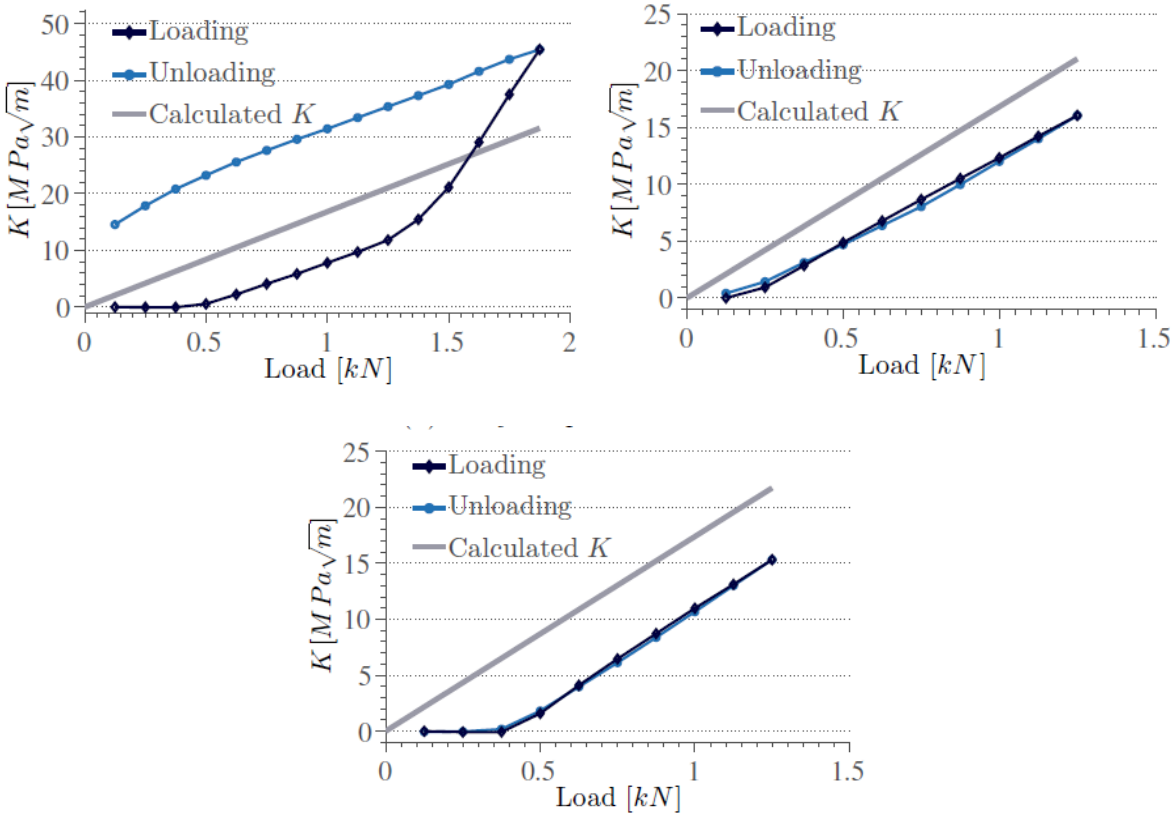

Figure 17. Experimental and theoretical variation of K with load (a) during the overload cycle, (b) for the cycle immediately after the overload and (c) 125 cycles after the overload.

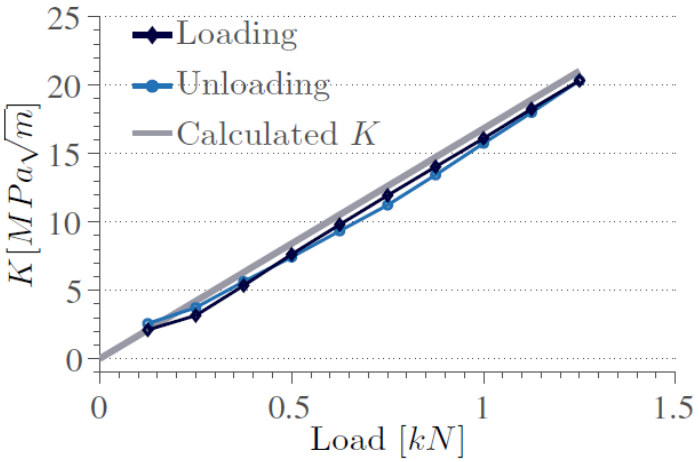

Figure 18. K vs Load plot for a cycle directly after a single overload cycle. The K value determined by displacement of points around the crack flanks is increased by the calculated K at 0.125 kN and the assumed crack tip is offset by 25 µm.

As well as looking at displacements and stress intensity factors during and after the overload, it is interesting to apply Pommier and Hamam's elastic/plastic model [25], as was done for constant amplitude loading. The results of this analysis are shown in Figure 19. In Figure 19(a) we show the K vs ρ plot for the overload cycle. As expected, there is a significant increase in ρ during loading. This is only partially reversed during unloading, in contrast to the constant amplitude results (Figure 10) which show almost closed K vs ρ loops for each cycle. Figure 19(b) shows the equivalent plot for the cycle immediately after the overload. Here, the cycle returns to an almost closed loop, with a shape which is much more similar to that predicted by the model (Figure 9). In particular, the initial decrease in ρ on loading, and initial increase on loading are now very small. This suggests that Pommier and Hamam's model is appropriate to cases with little or no crack closure, but may not correctly incorporate closure effects and the associated residual strain field at the crack tip.

Once the crack has grown away from the overload, the K vs ρ returns to the steady state. Figure 19(c) shows the values obtained for the cycle which is 125 cycles after the overload. This can be seen to be very similar to the pre-overload cycle shown in Figure 11(a). Finally, we should again make the point that the datum image for each cycle of results shown is that for minimum load. Hence, the loops shown in Figure 19 (a), (b), and (c) each start from (0,0). However, one sees from Figure 19(a) that there is both a residual K and a residual ρ after the overload. Hence a more realistic way of presenting the results might be thought to be to plot a number of successive cycles on a single diagram. This is done in Figure 19(d), which shows the cycle before overload, the overload cycle, and the cycle after

the overload on the same plot. This emphasises, for example, that both K and ρ remain positive in the cycle after the overload, when referenced to the pre-overload values.

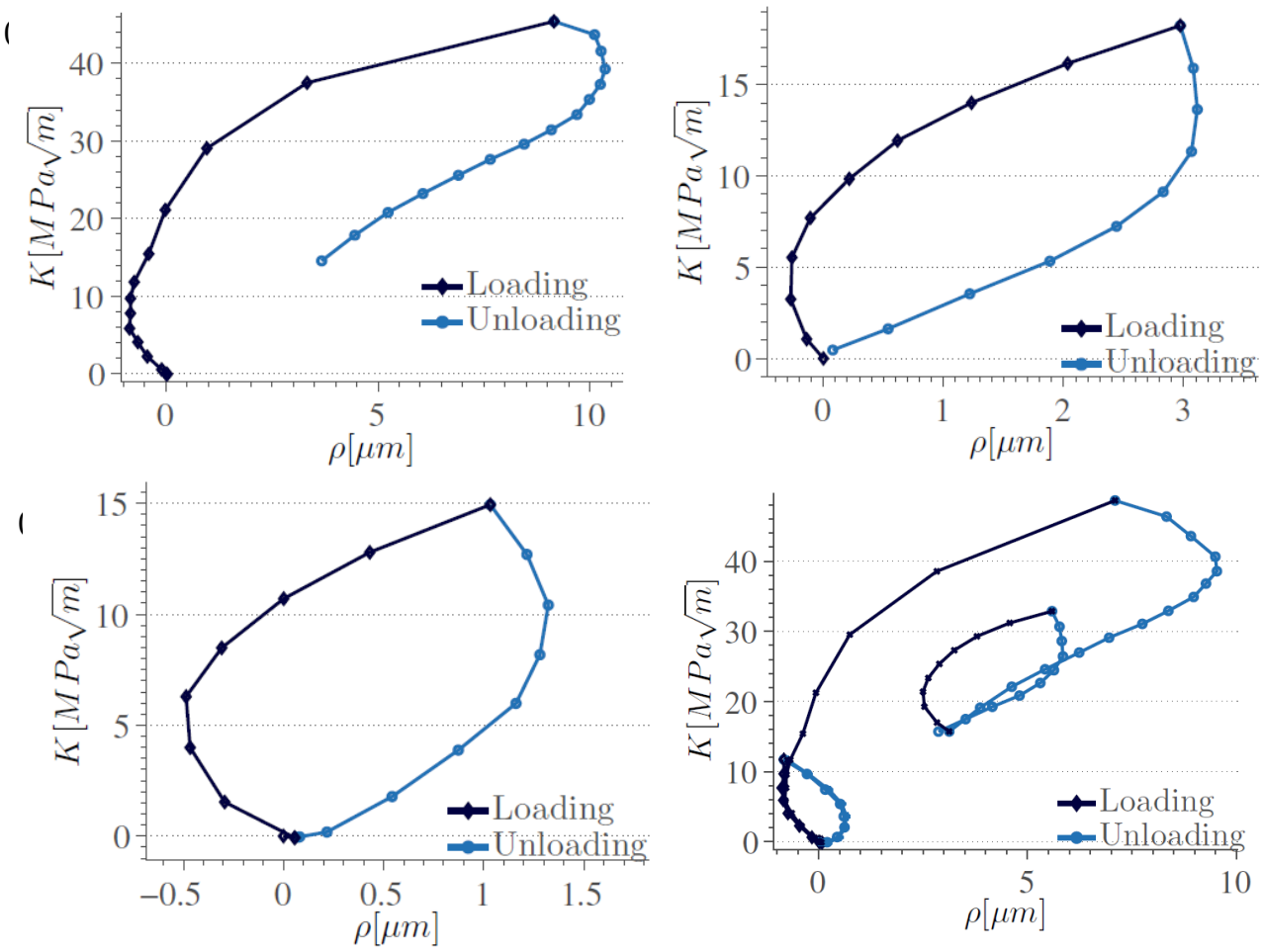

Figure 19. Variation of K and ρ (a) for the overload cycle (b) for the cycle immediately after the overload (c) for a cycle 125 cycles after the overload (d) pre-overload, overload, and post-overload plotted with the same datum.

5. Conclusions

The paper has presented a technique for in-situ loading of a small compact tension specimen in a scanning electron microscope. It has proved possible to take high quality images of the area close to the crack tip during complete loading cycles. Constant amplitude data are reported here, together with images from a single overload. Digital image correlation has been used to analyse the data using both an elastic and an elastic-plastic approach. The elastic approach models the measured displacements surprisingly well, although the fit is less good very close to the crack tip. An elastic-plastic approach provides a better fit, but there are still deficiencies in capturing deformations close to the tip. This may be partly because the existence of the process zone at the tip affects the displacements measured at

the grid locations, and these may no longer represent purely crack flank displacement. A more sophisticated elastic-plastic model is almost certainly in order to model the data more accurately, but the experiment has demonstrated the capability to measure displacements close to the crack tip which will be useful in calibrating a range of other models. The results from a single overload cycle are particularly interesting. During the overload, it is clear that significant plasticity takes place, and there is a large increase in crack tip opening displacement (characterised by the parameter ρ in Pommier and Hamam's model). This is likely to be associated with crack tip blunting. Immediately after the overload it is clear that the crack is always open to the tip, and the behaviour is much closer to that predicted by the model. By 125 cycles after the overload, the observed behaviour had returned to something very similar to that observed during the initial constant amplitude loading. There is no evidence of the increased closure post-overload that was observed in the macroscopic measurements [16]. However, this may be because the crack had not been propagated for a sufficient number of cycles after the overload. Although the DIC approach gives purely a surface measurement, the ability to study the near tip behaviour very close to the tip is extremely powerful, and the extraction of quantitative information is particularly useful. Use of the scanning electron microscope means that there is also the possibility of combining the measurements with other techniques such as electron backscatter diffraction, and this will form the basis of our further research in this area [27]. We have, of course, only tackled a very simple load case, and it is clear that more general loading will be much more challenging to interpret. However, the experimental tools outlined here provide an excellent basis for model validation, and in principle a more complex load history could be achieved using the Deben rig.

6. References

[1] Paris, P., Erdogan, F., A critical analysis of crack propagation laws, Jnl Basic Engineering, 85 (1963) 528-534.

[2] Marloff, R.H., Leven, M.M, Ringler, T.N., and Johnson, R.L., 'Photoelastic determination of stress intensity factors', Experimental Mechanics, 11(12) (1971), 529-539.

[3] Nurse, A.D., O'Brien, E.W., and Patterson, E.A., 'Stress intensity factors for cracks at fastener holes' Fatigue & Fracture of Engineering Materials & Structures, 17(7) (1994), 791-799.

[4] Rosakis, A.J., 'Analysis of the opical method of caustics for dynamic crack propagation', Engineering Fracture Mechanics, 13(1980), 331-347.

[5] Crosley, P.B., Mostovoy, S., and Ripling, E.J, 'An optical interference method for experimental stress analysis of cracked structures', Engineering Fracture Mechanics, 3(1971), 421-426.

[6] Dally, J.W., and Sanford, R.J, 'Strain-gage methods for measuring the opening mode stress intensity factor, K_I', Experimental Mechanics, 27(4) (1987), 381-388.

[7] Hild, F., Roux, S., 'Digital image correlation: from displacement measurement to identification of elastic properties – a review', Strain, 42(2) (2006), 69–80.

[8] McNeill, S.R., Peters, W.H., and Sutton, M.A., 'Estimation of stress intensity factor by digital image correlation', Engineering Fracture Mechanics, 28(1987), 101-112.
[9] Lopez-Crespo, P., Camas-Peña, D., Gonzalez-Herrara, A., Yates, J.R., Patterson, E.A., and Zapatero, J., 'Numerical and experimental analysis of crack closure', Key Engineering Materials, 385-387(2008), 369-372.
[10] Limodin, N., Rethore, J., and Buffiere, J.Y., 'Influence of closure on 3D propagation of fatigue cracks in a nodular cast iron investigated by X-Ray tomography and 3D volume correlation', Acta Materialia, 58 (2010), 2957 – 2967.
[11] Sutton, M.A., Zhao, W., McNeill, S.R., Helm, J.D., Piascik, R.S., and Riddell, W.T., 'Local crack closure measurements: Development of a measurement system using computer vision and a far-field microscope', pp145-156 of ,Advances In Fatigue Crack Closure Measurement And Analysis: Vol 2, Edited by: R.C. McClung, and J.C. Newman, ASTM STP 1343, 1999.
[12] Carroll, J., Efstathiou, C., Lambros, J., Sehitoglu, H., Hauber, B., Spottswood, S., and Chona, R., 'Investigation of fatigue crack closure using multiscale image correlation experiments', Engineering Fracture Mechanics, 76, 15 (2009), 2384-2398.
[13] Steuwer, A., Rahman, M., Shterenlikht, A., Fitzpatrick, M.E., Edwards, L. and Withers, P.J., 'The evolution of crack-tip stresses during a fatigue overload event', Acta Materialia, 58, 11(2010), 4039-4052.
[14] Nowell, D., Kartal, M.E., de Matos, P.F.P., Measurement and modelling of near-tip displacement fields for fatigue cracks in 6082 T6 aluminium, Proc. First I.J. Fatigue & FFEMS Joint Workshop, Forni di Sopra, Italy, March 7-9, 2011, Gruppo Italiano Frattura, 2011.
[15] Nowell, D., Kartal, M.E., de Matos, P.F.P., Digital image correlation measurement of near-tip fatigue crack displacement fields: constant amplitude loading and load history effects, Fatigue Fract. Engng Mater. Struct., 36 (2013) 3-13.
[16] Nowell, D., Kartal, M.E., and de Matos, P.F.P., Characterisation of crack tip fields under non-uniform fatigue loading, Proc. Second I.J. Fatigue & FFEMS Joint Workshop, Malaga, Spain, April 15-17, 2013, Gruppo Italiano Frattura, 2013.
[17] Nowell, D., O'Connor, S.J., and Dragnevski, K.L., 'Measurement and analysis of fatigue crack deformation on the macro- and micro-scale' Frattura ed Integrità Strutturale, 33 (2015) 1-7.
[18] de Matos, P.F.P., and Nowell, D., 'Experimental and numerical investigation of thickness effects in plasticity-induced fatigue crack closure', Int. Jnl Fatigue, 31(2009), 1795-1804.
[19] Eberl, C. Thompson, R., Gianola, R., Digital image correlation and tracking with Matlab, Matlab Central file exchange (2006) http://www.mathworks.co.uk/matlabcentral/fileexchange/12413-digital-image-correlation-and-tracking.
[20] Karolczuk, A., Kurek, M., and Łagoda, T. 'Fatigue life of aluminium alloy 6082 T6 under constant and variable amplitude bending with torsion', Journal of Theoretical and Applied Mechanics, 53, 2(2015), 421-430.
[21] Kammers, A.D., and Daly, S., 'Digital Image Correlation under Scanning Electron Microscopy: Methodology and Validation, Experimental Mechanics, 53, 1743-61, 2013.
[22] Irwin, G.R., Plastic zone near a crack and fracture toughness, Mechanical and Metallurgical Behavior, Proc. Seventh Sagamore Ordnance Materials Research Conference pp. IV-63 to IV-78, 1960.
[23] Westergaard, H.M., 'Bearing pressures and cracks', Trans. ASME, 61(1939), A49-53.
[24] Ewalds, H.L., and Wanhill, R.J.H., 'Fracture Mechanics', Delftse Uitgevers Maatschappij/Edward Arnold, 1984.
[25] Pommier, S., Hamam, R., Incremental model for fatigue crack growth based on a displacement partitioning hypothesis of mode I elastic-plastic displacement fields, Fatigue Fract. Engng Mater. Struct., 30 (2006) 582-598.
[26] Carroll, J.D., Abuzaid, W., Lambrose, J., and Sehitoglu, H., 'High resolution digital image correlation measurements of strain accumulation in fatigue crack growth', International Journal of Fatigue, 57(2013), 140–150.
[27] Salvati, E., O'Connor, S., Nowell, D., and Korsunsky, A.M., 'EBSD investigation of fatigue crack propagation past a crack closure due to overload', Proc. 5th International Conference on Crack Paths, Ferrara, Italy, 16-18 September, 2015.